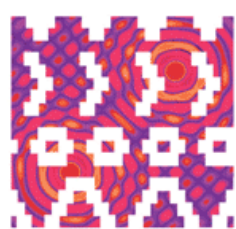


# CFA/VISHNO 2016

## Wave damping and evanescence: how to combine the spatial and temporal visions of the same problem?

E. Balmes, M. Rébillat et E. Arlaud

Arts et Metiers ParisTech / SDTools, 151 Bld de L'hôpital, 75013 Paris, France  
etienne.balmes@ensam.eu



LE MANS

It is proposed to analyze the forced response of periodic structures using a 2D Fourier transform using continuous time and discrete space. The simple example of compression waves is used to show that this response can be used to define poles in the wavenumber domain corresponding to evanescent waves or poles in the frequency domain corresponding to damped periodic modes. Link with classical computational methods based on FEM models of cells was done for both the periodic solution and wave based approach (SAFE, WFE). Two examples are analyzed in more detail: a simple train track model exhibiting a band-gap and the more complex case of a honeycomb panel where cell wall bending occurs within the band of interest.

## 1 Introduction

At the material level, damping is typically well taken into account by considering viscoelastic materials with a constant or frequency dependent complex modulus [1, 2] where the usual characterization is associated with the loss factor giving the ratio of dissipated energy per cycle over maximum strain energy. When performing modal analysis of finite structures [3] or system dynamics in general, damping is characterized by the damping ratio of poles associated with complex modes which gives a measure of amplitude decrease for each time period. This definition is for example the basis of the traditional logarithmic decrement method. When considering plane waves, the classical approach is to consider the forced response at a given frequency and characterize the effect of damping through the evanescence associated with the exponential decrease with space, as illustrated in [4] for example. Relating spatial evanescence and classical characterizations of modal damping ratio is however not direct and will be the focus of this paper.

When considering mono-dimensional wave propagation, the novel argument made in this paper is that it is useful to analyze 2D-transfer function in the angular frequency and wavenumber domains resulting from the Fourier transform of responses in time and space. The proposition can be seen as a specific post-processing of results computed using SAFE methods [5] for models that are continuous in space and WFE methods [6, 7, 4, 8] for spatially periodic structures, such as the tracks and honeycomb panels that will be used as examples here. In both cases, the 2D transfer is computed as a function of frequency. It is however useful to note that solvers for periodic solutions [9, 10, 11] are a completely different strategy to compute the same 2D transfer functions. In these methods the 2D transfer is computed at different wavenumbers.

Section 2 will analyze the base concepts associated with 2D transfer functions using the simple case of compression waves, illustrating in particular the relation between mode damping and wave evanescence and the specificities associated with responses that are sampled in space. Section 3 will then give a perspective on numerical strategies used in periodic and wave approaches. Finally, using FEM solutions implemented in SDT [12], section 4 will illustrate possible analyzes for a simple track model with a bandgap and a honeycomb panel considered in SHM applications [13].

## 2 Formulation for a continuous case

### 2.1 2D Fourier transforms in space and time

Considering a field  $g(x, t)$  depending on both time  $t$  and space  $x$ , the two-dimensional Fourier transform (2D-FT) is given by Eq. (1).

$$g(x, t) \xrightarrow{2D-FT} G(k, \omega) = \iint_{\mathbb{R}^2} g(x, t) e^{-ikx - i\omega t} dx dt \quad (1)$$

where  $k$  and  $\omega$  are the wavenumber and angular frequency.

A structure is said spatially periodic when it is composed of geometrically identical cells (labeled “slices” in this paper), generated by a translation in a predefined direction ( $x$  in the following work) from the reference slice.

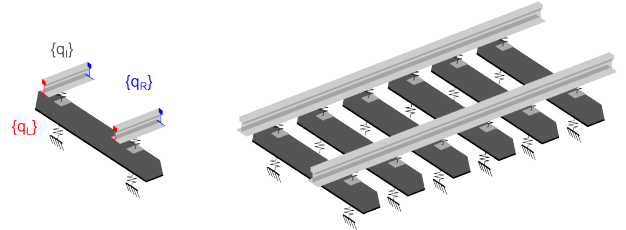


Figure 1: Sample spatially periodic structure

Using this geometric periodicity, any mechanical field of interest is known at a series of points associated with slice number  $n$  and position  $x_0$  within the reference slice, that is  $\tilde{g}(n, t, x_0) = g(x_0 + n\Delta x, t)$  with  $n \in [-\infty, \infty]$ . In that case, the two-dimensional discrete space Fourier transform (2D-DSFT) of  $\tilde{g}(n, t, x_0)$  is defined as

$$\tilde{g}(n, t, x_0) \xrightarrow{2D-DSFT} \tilde{G}(\kappa_c, \omega, x_0) = \sum_{n=-\infty}^{+\infty} \int_{\mathbb{R}} \tilde{g}(n, t, x_0) e^{-i\kappa_c n - i\omega t} dt \quad (2)$$

where  $\kappa_c$  and  $\omega$  are the dimensionless wavenumber and angular frequency. By definition, the function  $\tilde{G}$  is  $2\pi$  periodic in  $\kappa_c$ . It is useful to note that the spatial transform thus built is often referred to as Floquet transform. The conventions used in this work regarding this spatial transform are the following

- $\kappa_c$  is the wavelength or spatial periodicity in number of cells, so  $\kappa_c \in [1, \infty]$ . The physical wavelength  $\lambda$  in length unit is then given by  $\lambda = \kappa_c \times \Delta x$
- The wavenumber  $\kappa_c$  in rad/number of cells is then given by  $\kappa_c = 2\pi/\kappa_c$ , so  $\kappa_c \in [0, 2\pi]$ .

The inverse spatial transform allows recovery of the physical field  $g$  based on its wave domain values  $\tilde{G}(\kappa_c, \omega, x_0)$ :

$$g(x_0 + n\Delta x, t) = \frac{1}{2\pi} \int_0^{2\pi} \tilde{G}(\kappa_c, \omega, x_0) e^{i\kappa_c n} d\kappa_c. \quad (3)$$

### 2.2 2D transfer functions for compression

The focus is now put on a simple example involving longitudinal waves propagating in a homogeneous material.

The wave propagation equation linking the applied force  $f(x, t)$  and the resulting displacement  $u(x, t)$  is

$$\rho \frac{\partial^2 u(x, t)}{\partial t^2} - E \frac{\partial^2 u(x, t)}{\partial x^2} = f(x, t) \quad (4)$$

with  $\rho$  the mass density of the considered material and  $E$  its Young modulus. Taking the 2D-FT of Eq. (4) leads to a spatio-temporal transfer function

$$\frac{U(k, \omega)}{F(k, \omega)} = \frac{1}{-\rho\omega^2 + Ek^2} \quad (5)$$

whose denominator corresponds to well known dispersion equation, which relates frequencies and wavelengths.

The classical point of view of the literature on wave propagation is the case where the applied force  $f(x, t)$  is spatially localized at  $x = 0$  and temporally corresponds to an harmonic excitation at angular frequency  $\omega$ . This force and its 2D-FT can then be expressed as

$$f(x, t) = F_0 e^{i\omega_0 t} \delta(x) \xrightarrow{2D-FT} F(k, \omega) = F_0 \delta(\omega - \omega_0) \quad (6)$$

with  $F_0$  the force amplitude and  $\delta(\cdot)$  the Dirac distribution defined as the neutral element of the convolution operator. As a consequence of Eq. (5), the response  $u(x, t)$  can then be recovered in the time/space domain as

$$u(x, t) = \iint_{\mathbb{R}^2} U(k, \omega) e^{ikx+i\omega t} dk d\omega = U_0 e^{\alpha(\omega_0)|x|} e^{i\omega_0 t} \quad (7)$$

with  $U_0 = \frac{-F_0}{2\alpha(\omega_0)E}$  and  $\alpha(\omega_0)$  such that  $\Re(\alpha(\omega_0)) \leq 0$  and

$$\alpha(\omega_0)^2 = -\frac{\rho\omega_0^2}{E}.$$

In later sections, periodic structures will be considered and the displacement will be only considered at discrete locations  $x = x_0 + n\Delta x$ . The expression of the corresponding series is:

$$\tilde{u}(n, t) = u(n\Delta x, t) = U_0 e^{\alpha(\omega_0)\Delta x|n|} e^{i\omega_0 t} \quad (8)$$

and the 2D-DSFT of the transfer function linking  $\tilde{U}(\kappa_c, \omega)$  and  $\tilde{F}(\kappa_c, \omega)$  is given by

$$\frac{\tilde{U}(\kappa_c, \omega)}{\tilde{F}(\kappa_c, \omega)} = \frac{-1}{2\alpha(\omega)E} \frac{1 - e^{-2\alpha(\omega)\Delta x}}{(1 - e^{-\alpha(\omega)\Delta x+i\kappa_c})(1 - e^{-\alpha(\omega)\Delta x-i\kappa_c})} \quad (9)$$

Figure 2 illustrates the 2D-DSFT of the compression problem. At low frequencies/wavenumbers, the shapes of (5) and (9) show a classical single mode resonance at a wavenumber. The difference becomes clear when the wavelength reaches  $\Delta x$  so that a wavenumber alias starts to appear in the 2D-DSFT.

A second point of view is to compute all frequencies at a given wavelength. One considers a force  $f(x, t)$  that temporally localized at  $t = 0$  and spatially corresponds to an harmonic solicitation at a wavenumber  $k_0$ . The 2D-FT of this force is given by

$$f(x, t) = F_0 e^{ik_0 x} \delta(t) \xrightarrow{2D-FT} F(k, \omega) = F_0 \delta(k - k_0) \quad (10)$$

Following the previous approach, the response in the  $(x, t)$  domain is given by

$$u(x, t) = U_0 e^{ik_0 x} e^{\lambda(k_0)t} \quad (11)$$

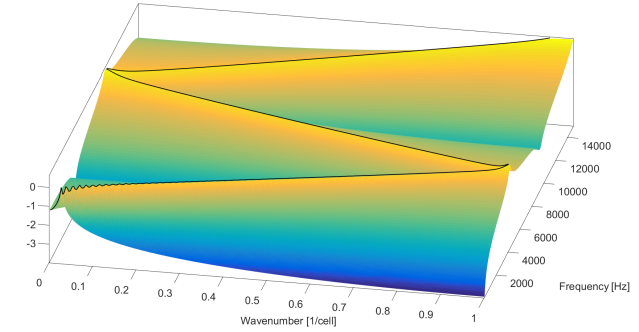


Figure 2: Transfer function of compression waves in the frequency-wavenumber domain as given by Eq. (9) and Eq. (13).

with  $U_0 = \frac{-F_0}{2\lambda(k_0)\rho}$  and  $\lambda(k_0)$  such that  $\Re(\lambda(k_0)) \leq 0$  and

$$\lambda(k_0)^2 = -\frac{Ek_0^2}{\rho}$$

If this displacement is known only at discrete locations  $x = n\Delta x$  in space, the solution is given as

$$\tilde{u}(n, t) = u(n\Delta x, t) = U_0 e^{ik_0 n \Delta x} e^{\lambda(k_0)t} \quad (12)$$

and the 2D-DSFT of the transfer function linking  $\tilde{U}(\kappa_c, \omega)$  and  $\tilde{F}(\kappa_c, \omega)$  is obtained as

$$\frac{\tilde{U}(\kappa_c, \omega)}{\tilde{F}(\kappa_c, \omega)} = \frac{1}{\rho} \sum_{n=-\infty}^{+\infty} \frac{1}{-\omega^2 + [\lambda(\kappa_c + 2\pi n)]^2} \quad (13)$$

which is equal to the 2D-DSFT computed in Eq. (9) and shown in Fig. 2. The interest of using either formulas is in numerical strategies for periodic models with more degrees of freedom that will be detailed in section 3.

### 2.3 Effect of damping

The usual representation of material damping is the use of a complex, possibly frequency dependent, Young modulus

$$E = E_0(1 + i\eta) = E_0 [1 + i\tan(\delta)] = |E|e^{i\delta} \quad (14)$$

Given the notations of Eq. (14), the following expressions are obtained for  $\alpha$  and  $\lambda$

$$\alpha(\omega) = \omega \sqrt{\frac{\rho}{|E|}} \left( \zeta - i \sqrt{1 - \zeta^2} \right) \quad (15)$$

$$\lambda(k) = k \sqrt{\frac{|E|}{\rho}} \left( \zeta - i \sqrt{1 - \zeta^2} \right) \quad (16)$$

with  $\zeta = \sin(\delta/2)$ . In this case, the propagation is non dispersive and the damping and evanescence ratio are identical.

When considering values discretized in space aliasing occurs as shown by Figure 2. The experimentally available pole  $\alpha_{XP}(\omega)$  in the wavenumber domain thus verifies

$$\alpha_{XP}(\omega)\Delta x = \Re(\alpha(\omega)\Delta x) + i|\Im(\alpha(\omega)\Delta x) - 2L\pi| \quad (17)$$

with  $L$  the only integer such that  $|\Im(\alpha(\omega)\Delta x) - 2\pi L| \in [0 \pi]$ .

Furthermore, when considering the angular frequency domain, an infinity of poles have to be considered. They are given by

$$\lambda_n(\kappa_c) = \lambda(\kappa_c + 2\pi n)$$

However, in practice only a few of them will really influence the 2D-DSFT and usual modal truncation and static correction methods can be used.

### 3 Structures with geometric periodicity

In practical cases, one will need to consider finite element models of the cell. This section will thus show how harmonic responses in the spatial and time domain have both been used to introduce optimized solvers.

#### 3.1 Periodic solutions in the spatial domain

A key property of periodic systems, see for example [9], is that for excitations at a given wavelength, described as a field on the nominal cell  $U(x_0, \kappa_{cx})$  associated with a single wavenumber  $\kappa_{cx}$ , the only response occurs at the same wavelength  $\kappa_{cx}$  provided that the geometry and model properties are strictly periodic. A large FEM problem with repeated slices can thus be decomposed in a series of independent problems for single wavenumbers, which correspond to periodic solutions.

For a solution with a single wavenumber  $\kappa_{cx}$ , the field is simply equal to

$$u(x_0 + n\Delta x) = \Re(U(x_0, \kappa_{cx})e^{ik_{cx}n}), \quad (18)$$

which will be used to compute the periodic solutions.

In the case of structures represented as FE models, the continuous displacement in the nominal cell  $u(x_0)$  is discretized and replaced by a vector  $\{q\}$  of Degrees Of Freedom (DOF) values.

To ensure the displacement continuity between adjacent periodic cells, a continuity condition must be introduced. The displacement on the left boundary of one cell has to be equal to the one of the preceding cell right edge, thus  $\{q_{left}(n\Delta x)\} = \{q_{right}((n-1)\Delta x)\}$ . Following the definition given in the previous section,  $\{q_n\}$  represents all the displacements at the DOF of the cell number  $n$ . For each cell, the observation matrices  $[c_l]$  and  $[c_r]$  can then be defined to extract on the whole DOFs the ones corresponding to respectively left and right boundaries. These matrices are the same for all cells if the domain is meshed regularly.

For a periodic response associated with a single wavenumber, taking into account Eq. (18), the continuity condition can be written as  $[c_l]\{Q(\kappa_{cx}, \omega)\} = [c_r]\{Q(\kappa_{cx}, \omega)\} e^{-2ik_{cx}}$  which, differentiating real and imaginary parts, leads to

$$[C(\kappa_{cx})] \begin{Bmatrix} \text{Re}(Q(\kappa_{cx}, \omega)) \\ \text{Im}(Q(\kappa_{cx}, \omega)) \end{Bmatrix} = 0, \quad (19)$$

with

$$[C(\kappa_{cx})] = \begin{bmatrix} [c_l] - \cos(\kappa_{cx})[c_r] & -\sin(\kappa_{cx})[c_r] \\ \sin(\kappa_{cx})[c_r] & [c_l] - \cos(\kappa_{cx})[c_r] \end{bmatrix}.$$

For an external force  $\{f\}$  applied to the system,  $s$  being the Laplace variable, the first step is to compute the Floquet (spatial Fourier) transform of the load  $F(\kappa_{cx}, s)$ . Then the

equations of motion, which are known to be decoupled for each wavenumber, take the frequency domain form

$$[Z(\omega)]\{Q(\kappa_{cx}, \omega)\} = \{F(\kappa_{cx}, \omega)\}, \quad (20)$$

where  $Z(\omega) = -M\omega^2 + K$  is the dynamic stiffness matrix. This matrix contains mass  $M$  as well as stiffness and damping in the matrix  $K$ . The matrix  $K$  can take into account hysteretic damping (constant imaginary part of  $K$ ) or viscoelastic contributions (frequency and temperature dependent  $K(\omega)$ ), see [2].

Since the frequency response can be complex in the spatial domain, it is necessary to distinguish real and imaginary parts of the spatial transform. The equations actually solved are thus

$$\begin{bmatrix} Z(\omega) & 0 \\ 0 & Z(\omega) \end{bmatrix} \begin{Bmatrix} \text{Re}(\{Q(\kappa_{cx}, \omega)\}) \\ \text{Im}(\{Q(\kappa_{cx}, \omega)\}) \end{Bmatrix} = \begin{Bmatrix} \text{Re}(F(\kappa_{cx}, \omega)) \\ \text{Im}(F(\kappa_{cx}, \omega)) \end{Bmatrix}, \quad (21)$$

with (19) verified.

Solution of a linear system Eq. (21) with constraint (19) is here obtained by elimination. The continuity condition is thus taken into account by first seeking a basis  $T$  of  $\ker([C(\kappa_{cx})])$ . Then this basis is used to find the solution of the constrained problem

$$([T]^T [Z(\kappa_{cx}, \omega)] [T]) \{Q(\kappa_{cx}, \omega)\} = [T]^T \{F(\kappa_{cx}, \omega)\}. \quad (22)$$

Solving directly this problem can be fairly long as it requires inversion of the constrained dynamic stiffness  $T^T Z(\omega) T$  at each desired frequency. Modal synthesis methods which combine modes and static corrections for loads, and possibly viscoelastic loads [14], are thus preferred here.

To analyze damping, one will seek to compute poles in the frequency domain (of the form Eq.(16)) which will correspond to the classical computation of complex modes

$$(T^T [K + (\lambda_j(\kappa_{cx}))^2 M] T) \{\psi_j(\kappa_{cx})\} = 0. \quad (23)$$

and use an expression of the 2D-DSFT of the form Eq.(13).

#### 3.2 Periodic solutions frequency domain: WFE

Taking the point of view of a harmonic response in the time domain, the equation of motion of a given slice  $k$  can be written as

$$\begin{bmatrix} Z_{LL}(\omega) & Z_{LI} & Z_{LR} \\ Z_{IL} & Z_{II} & Z_{IR} \\ Z_{RL} & Z_{RI} & Z_{RR} \end{bmatrix} \begin{Bmatrix} q_L(\omega) \\ q_I(\omega) \\ q_R(\omega) \end{Bmatrix} = \begin{Bmatrix} F_L(\omega) \\ 0 \\ F_R(\omega) \end{Bmatrix} \quad (24)$$

where it is possible [6] to distinguish states of sections  $\{q\}_k$  and internal states  $q_I$  which are entirely defined by the second row of (24) (a step known as dynamic condensation of the internal states). The remaining equations can be reformulated as a transition matrix problem

$$\begin{Bmatrix} q \\ F \end{Bmatrix}_{k+p} = [S]^p \begin{Bmatrix} q \\ F \end{Bmatrix}_k \quad (25)$$

where  $S$  is a linear operator so that its power is more efficiently computed through diagonalization

$$[S(\omega)]^p = \sum_j \{U_j(\omega)\} (\mu(\omega))_j^p \{V_j(\omega)\}^T \quad (26)$$

in a series of propagating waves. The literature on WFE methods [6, 7, 4, 8] addresses the proper way of computing the eigenvalues and eigenvectors of the transition matrix while properly accounting for symmetry properties resulting in inverse eigenvalues for left and right going waves and avoiding scaling issues associated with the different nature of displacements and loads appearing in the state vector.

For the sake of the present paper, the key aspect is that the response at a given slice is of the generic form

$$\{u(n, \omega)\} = \sum_j \mu_j^p \{u_j(\omega)\} \quad (27)$$

For the case of infinite structure with a point load at position  $x = 0$ , a finite solution necessarily only has left going waves ( $|\mu_j| > 1$ ) on the left and right going waves ( $|\mu_j| < 1$ ) on the right. As a result, one actually has a solution of the form

$$\{u(n, \omega)\} = \sum_j e^{\alpha_j n} \{u_j(\omega)\} \text{ with } \alpha_j = \ln(\mu_j) \quad (28)$$

whose Fourier/Floquet transform is given by

$$\{u(k, \omega)\} = \sum_j \frac{u_j(\omega)(1 - \mu_j^2)}{(1 - e^{\alpha_j(\omega) - ik})(1 - e^{\alpha_j(\omega) + ik})} \quad (29)$$

which clearly has the form(9).

## 4 Applications

### 4.1 Sample application with a bandgap: simplified track model

In railway research, a widespread approach to get dynamic information on the global track behavior is to perform a receptance test [15]. That is to measure transfer function between displacement under impact and force at the rail level. This test characterizes the global behavior of track for a range of frequencies and allows identifying the main resonances of the structure. It characterizes the structure sensitivity to vibrations [16] and the dynamic flexibility of the track [17]. This test is frequently used in numerical studies to adjust numerical model properties [18, 19, 20] or give insights on the wave propagation in the substructure layers, as used by [21] to assess soft soil influence.

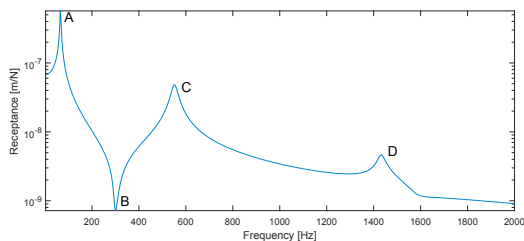


Figure 3: Receptance associated with an impact on the rail.

The Fourier transform of the forced response of the railway track modeled as displayed in Figure 1 in the wavenumber / frequency domain is shown in Figure 4. The black-lines indicate the values of frequencies found by

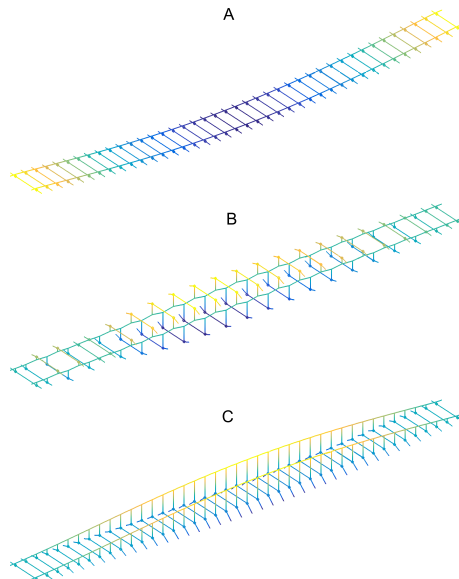


Figure 5: Finite length modes associated with points A,B,C

computation of an elastic dispersion diagram. The main low frequency peak, point A of Figure 3, at 15 Hz is associated with the track resonance on the soil. The associated mode shape is shown for a two rail track in Figure 5a. The second feature, point B of the receptance is found near 290 Hz. The nearest periodic mode, shown in 5b corresponds to an alternating motion of adjacent sleepers leading to very small motion of the rail. This is a classical bandgap since no possible periodic mode frequency exists until point C, which corresponds to a resonance of the rail on the pads, as displayed in 5c with little motion of the sleepers. Finally the so called pin-pin mode occurs near 1400 Hz and corresponds to the frequency at which the wave propagation in the rail gets aliased. At that frequency the rail has opposite phases for adjacent sleepers.

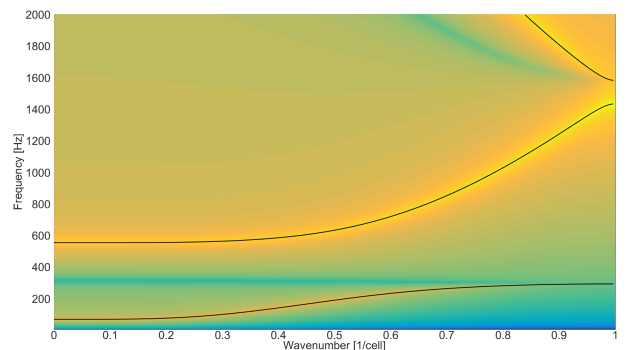


Figure 4: Amplitude of the forced response of a periodic track in the wavenumber/frequency domain.

These four characteristic points are classical features of railway track receptance as stated by [16].

Finally an important objective of this study was to analyze the relation between attenuation along the track and damping. To properly analyze the result in relation with the previous responses, rather than classically presenting the real and imaginary parts of  $\alpha_j$ , the choice is made here to represent the frequency and wave number and use color coding to display in Figure 6 the evanescence ratio as a value

between 0 (fully dissipative) and 1 (purely propagative). The chosen colormap emphasizes the propagating modes with peaks visible in 2D transfer Figure 4, corresponding to waves with a small evanescence ratio. It also illustrates that evanescence depends on the group velocity estimated by  $\partial\omega_j/\partial k$ .

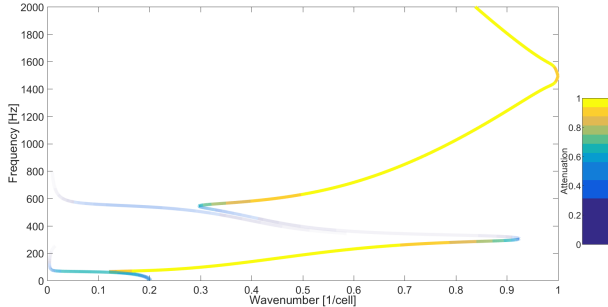


Figure 6: Track attenuation as a function of frequency and wave number.

## 4.2 Honeycomb panel

Now considering the case of a honeycomb panel, one is interested in understanding propagation of in-plane "membrane modes" in the skins (often referred to as the S0 waves in the Lamb wave literature). The base cell shown in Figure 1 is modeled using 556 quadratic volume elements for 11000 DOF including 1350 interface nodes making the cost of WFE approaches significant. To focus on in-plane waves a symmetric in-plane loading of the top and bottom skins is applied and the transfer function to the mean in-plane response on the two skins is shown in Figure 7.

The black lines on the plot show the dispersion diagram clearly show the high number of propagating waves. Bending, indicated as point (a), occurs first but is not excited by the considered load and thus does not lead to peak in the 2D-DSFT transfer. A large number of slowly propagating wall bending modes, point (b) for example, occur at relatively low frequencies due to the small thickness of the honeycomb walls.

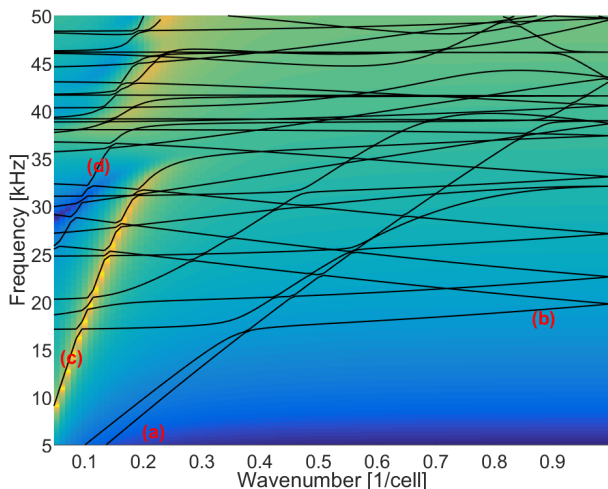


Figure 7: Transfer associated with an in plane load in the frequency-wavenumber domain.

The in-plane wave of interest is indicated by point (c) and

its evolution with frequency is clearly indicated by the peak of the transfer function. The second mode propagating with the same group velocity is the anti-symmetric in-plane mode (d). An interesting feature of this response is the existence of a band-gap between 33 and 40 kHz. As for the track model, this gap is associated with distributed resonating substructures which here correspond to the honeycomb wall bending.

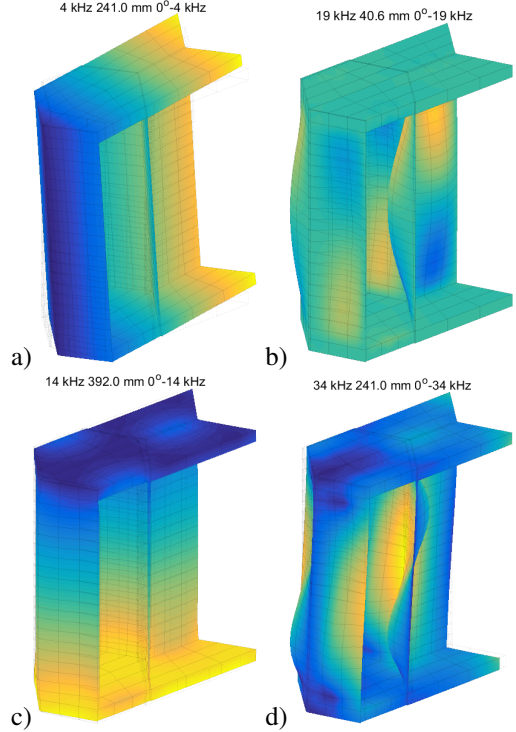


Figure 8: Sample wave shapes. a) bending mode, b) first wall bending, c) symmetric in-plane compression, d) anti-symmetric in-plane compression

## 5 Conclusion

The paper proposed to analyze the forced response of periodic structures using a 2D Fourier transform using continuous time and discrete space. The simple example of compression waves was used to show that this response could be used to define poles in the wavenumber domain corresponding to evanescent waves or poles in the frequency domain corresponding to damped periodic modes. Link with classical computational methods based on FEM models of cells was done for both the periodic solution and wave based approach.

Two examples were analyzed in more detail: a simple train track model exhibiting a band-gap and the more complex case of a honeycomb panel where cell walls bending occurs within the band of interest. Damping could be analyzed both in terms of modal damping and wave evanescence with the effect of group velocity needing to be analyzed further. Other ongoing work is related to model reduction in the periodic approach allowing later use of WFE or transients as in [11].

## References

- [1] A. Nashif, D. Jones, J. Henderson, *Vibration Damping*, John Wiley and Sons, 1985.
- [2] E. Balmes, Viscoelastic vibration toolbox, User Manual, SDTools, 2004-2013.  
URL <http://www.sdttools.com/pdf/visc.pdf>
- [3] W. Heylen, S. Lammens, P. Sas, *Modal Analysis Theory and Testing*, KUL Press, Leuven, Belgium, 1997.
- [4] M. Collet, M. Ouisse, M. Ruzzene, M. Ichchou, Floquet-Bloch decomposition for the computation of dispersion of two-dimensional periodic, damped mechanical systems, *International Journal of Solids and Structures* 48 (20) (2011) 2837–2848. doi:[10.1016/j.ijsolstr.2011.06.002](https://doi.org/10.1016/j.ijsolstr.2011.06.002).
- [5] L. Gavrić, Computation of propagative waves in free rail using a finite element technique, *Journal of Sound and Vibration* 185 (3) (1995) 531–543.  
URL <http://www.sciencedirect.com/science/article/pii/S0022460X85703987>
- [6] W. X. Zhong, F. W. Williams, On the direct solution of wave propagation for repetitive structures, *Journal of Sound and Vibration* 181 (3) (1995) 485–501.  
URL [sciencedirect.com/science/article/pii/S0022460X85701538](http://www.sciencedirect.com/science/article/pii/S0022460X85701538)
- [7] B. Mace, R., D. Duhamel, M. Brennan, J., L. Hinke, Finite element prediction of wave motion in structural waveguides, *J. Acous. Soc. America* (2005) 2835–2843.  
URL [10.1121/1.1887126](https://doi.org/10.1121/1.1887126)
- [8] J.-M. Mencik, New advances in the forced response computation of periodic structures using the wave finite element (WFE) method, *Computational Mechanics* 54 (3) (2014) 789–801. doi:[10.1007/s00466-014-1033-1](https://doi.org/10.1007/s00466-014-1033-1).
- [9] A. Sternchüss, E. Balmes, P. Jean, J. Lombard, Reduction of Multistage disk models : application to an industrial rotor, *Journal of Engineering for Gas Turbines and Power* 131, paper Number GT2008-012502.  
URL <http://dx.doi.org/10.1115/1.2967478>
- [10] H. Chebli, D. Clouteau, L. Schmitt, Dynamic response of high-speed ballasted railway tracks: 3D periodic model and in situ measurements, *Soil Dynamics and Earthquake Engineering* 28 (2) (2008) 118–131. doi:[10.1016/j.soildyn.2007.05.007](https://doi.org/10.1016/j.soildyn.2007.05.007).
- [11] E. Arlaud, S. C. D. Aguiar, E. Balmes, Numerical study of railway track dynamics: Case of a transition zone, in: *Proceedings Railways*, Cagliari, 2016.
- [12] E. Balmes, Structural Dynamics Toolbox (for use with MATLAB), SDTools, Paris, September 1995-2014.  
URL <http://www.sdttools.com/help/sdt.pdf>
- [13] C. Fendzi, N. Mechbal, M. Rébillat, M. Guskov, G. Coffignal, A general bayesian framework for ellipse-based and hyperbola-based damage localization in anisotropic composite plates, *Journal of Intelligent Material Systems and Structures* 27 (3) (2016) 350–374. doi:[10.1177/1045389X15571383](https://doi.org/10.1177/1045389X15571383).
- [14] E. Balmes, S. Germes, Design strategies for viscoelastic damping treatment applied to automotive components, IMAC, Dearborn.  
URL [www.sdttools.com/pdf/imac04\\_damp.pdf](http://www.sdttools.com/pdf/imac04_damp.pdf)
- [15] G. Lombaert, G. Degrande, J. Kogut, S. François, The experimental validation of a numerical model for the prediction of railway induced vibrations, *Journal of Sound and Vibration* 297 (3-5) (2006) 512–535. doi:[10.1016/j.jsv.2006.03.048](https://doi.org/10.1016/j.jsv.2006.03.048).
- [16] A. P. D. Man, Dynatrack: A survey of dynamic railway track properties and their quality, Phd, Delft University (2002).
- [17] K. Knothe, Y. Wu, Receptance behaviour of railway track and subgrade, *Archive of Applied Mechanics* 68 (7-8) (1998) 457–470. doi:[10.1007/s004190050179](https://doi.org/10.1007/s004190050179).
- [18] S. Kaewunruen, A. M. Remennikov, Field trials for dynamic characteristics of railway track and its components using impact excitation technique, *NDT & E International* 40 (7) (2007) 510–519. doi:<http://dx.doi.org/10.1016/j.ndteint.2007.03.004>.
- [19] A. C. C. A. Ribeiro, Transições aterro - estrutura em linhas ferroviárias em alta velocidade: Analise experimental e numérica, Phd, FEUP (2012).
- [20] H. Verbraken, G. Degrande, G. Lombaert, B. Stallaert, V. Cuellar, Benchmark tests for soil properties, including recommendations for standards and guidelines, Project no. scp0-ga-2010-265754 rivas, RIVAS D1.11 (2013).
- [21] E. G. Berggren, A. M. Kaynia, B. Dehlbom, Identification of substructure properties of railway tracks by dynamic stiffness measurements and simulations, *Journal of Sound and Vibration* 329 (19) (2010) 3999–4016. doi:[10.1016/j.jsv.2010.04.015](https://doi.org/10.1016/j.jsv.2010.04.015).